Journal of Thermal Analysis and Calorimetry (2023) 148:4119–4127
https://doi.org/10.1007/s10973-023-11990-z

Oxidation behavior of Ti_2AlC MAX-phase foams in the temperature range of 600–1000 °C

Marek Potoczek[1] · Jarosław Dąbek[2] · Tomasz Brylewski[2]

Received: 7 September 2022 / Accepted: 22 January 2023 / Published online: 21 February 2023

Abstract
The isothermal oxidation behavior of Ti_2AlC gel-cast foams with an almost completely open porosity of 87 vol% was investigated in the temperature range of 600–1000 °C, in static air, and for exposure times of up to 6.5 h. It was found that the oxidation process obeyed the parabolic rate law. The determined parabolic oxidation rate constants were low, indicating that the material's resistance to oxidation at high temperatures was very good, especially given its highly porous form. The nature of the scale formed on the strut surface of Ti_2AlC foams changed significantly with increasing oxidation temperature. After oxidation at 600 °C, gaps/cracks were observed between Ti_2AlC layers on the strut surface, and the oxidation products were mixed Ti and Al oxides. At 700–800 °C, the scales were integrated and composed of Ti and Al oxides. At 900–1000 °C, the oxidation products were composed of large elongated plates of TiO_2 (rutile) and small, needle-like Al_2O_3 (corundum) grains.

Keywords Thermogravimetry · Gaseous corrosion · Porosity · Carbides · Ti_2AlC · Foams

Introduction

Ti_2AlC is a member of the MAX-phase family of layered ternary carbides and nitrides. The typical formula for this family is $M_{n+1}AX_n$ ($n = 1$–3), where M is an early transition metal, A is an A-group element, and X is C, N, or both [1, 2]. Due to their layered structure and combination of ionic, covalent, and metallic bonds, MAX phases exhibit desirable features that are intermediate between those of ceramics and metals [3, 4]. With ceramics, they share a high melting point, high resistance to oxidation, and low density, while their resemblance to metals stems from their machinability and ductility as well as electrical and thermal conductivity. The reason why MAX materials exhibit such properties is that they form strong covalent–ionic M-X bonds and weak metallic M-A bonds inside their layered hexagonal structures. These properties make them ideal candidates for specific high-temperature applications [5]. Examples of high-temperature applications of dense MAX phases include electrical heating elements [6], gas burner nozzles in corrosive environments, high-temperature bearings [7], cladding materials in lead-cooled fast-breeder nuclear reactors [8], and high-temperature electrodes [9]. The MAX phases that are suitable for high-temperature (900–1400 °C) applications are Ti_2AlC, Ti_3AlC_2, and Cr_2AlC; all of these phases have the ability to form an external α-Al_2O_3 layer that exhibits good adhesion and protects against further inward oxygen diffusion at high temperatures [1, 10]. Ti_2AlC is known to exhibit the highest oxidation resistance and can withstand 10,000 thermal cycles with temperatures reaching 1350 °C without spallation or cracking of the outer protective Al_2O_3 layer. There are certain discrepancies in the literature that describes the oxidation kinetics of dense Ti_2AlC. Some authors postulated a cubic rate law, while others are a parabolic rate one [1, 11]. Eventually, it was determined that grain boundary diffusion is responsible for the alumina scale growth. Consequently, cubic oxidation kinetics gained acceptance [12]. In spite of this, it has been recently demonstrated that cubic oxidation kinetics is solely due to the growth of a compact Al_2O_3. Parabolic kinetics corresponds with the formation of a discontinuous alumina scale, which allows for constant inward oxygen diffusion [13, 14]. Furthermore, the oxidation response is highly dependent on

✉ Marek Potoczek
potoczek@prz.edu.pl

[1] Faculty of Chemistry, Rzeszow University of Technology, Al. Powstańców Warszawy 12 Av., 35-959 Rzeszów, Poland

[2] Faculty of Materials Science and Ceramics, AGH University of Science and Technology, Al. Mickiewicza 30, 30-059 Kraków, Poland

such factors as follows: particle size, orientation, secondary phases, and surface roughness [13–15].

There is a considerable amount of experimental data on the structure, properties, and processing of dense Ti_2AlC and other MAX phases in this form. However, the data published on the porous forms of these materials are scarce [16–27]. For example, porous Ti_2AlC is an attractive material for high-performance applications such as electrode materials for harsh chemical environments, microbial fuel cells (MFCs), and solar volumetric collectors [16, 17]. As in the case of dense Ti_2AlC materials, good high-temperature oxidation behavior is essential. However, the literature includes few detailed studies on the oxidation behavior of highly porous MAX phases [28–31]. Tsipast et al. [28] studied the oxidation behavior of porous Ti_2AlC and Ti_3SiC_2 produced by means of the space-holder method and for a porosity ranging from 20 to 60 vol%. Ti_2AlC was oxidized at 1000 °C, while Ti_3AlC_2 at 900 °C via a non-continuous method. All tested samples of Ti_2AlC and Ti_3SiC_2 were resistant to oxidation and thermal shock in cyclic tests of 24 h, conducted for a total of 240 h at 1000 °C (Ti_2AlC) and 900 °C (Ti_3SiC_2); this resistance stemmed from the protective oxide layers that formed on the surface of the material. These layers had a dual nature in both materials. In Ti_2AlC, an outer layer of TiO_2 and an inner layer of Al_2O_3 had formed; Ti_3SiC_2 had an outer layer of TiO_2 and an inner layer of TiO_2 and SiO_2. The protective inner layers were dense, highly adhesive, crack-free, and exhibited high resistance when exposed to thermal cycling. Zhang et al. [29] studied the oxidation of commercial Ti_2AlC MAX-phase powders at temperatures in the range of 200–1000 °C. This result indicated that Ti_2AlC had good oxidation resistance—even in powder form. A considerable degree of oxidation was observed at 600 °C; the powders oxidized at this temperature contained rutile with minor amounts of anatase. At 800 °C, α-Al_2O_3 was detected, while anatase transformed into rutile. At 1000 °C, the Ti_2AlC powders were fully oxidized and consisted of rutile and α-Al_2O_3. Kong et al. [30] studied the oxidation behavior of high-purity non-stoichiometric Ti_2AlC_X ($x = 0.69$) powders in flowing air at temperatures ranging from 400 to 900 °C. The oxidation of fine Ti_2AlC powders with a grain size of about 1 µm starts at300 °C and is complete by 980 °C, whereas when grain size is around 10 µm, the corresponding temperatures increase to 400 and 1040 °C, respectively. It was stated that the oxidation of nonstoichiometric Ti_2AlC_x ($x = 0.69$) powders is controlled by a surface reaction in the range of 400–600 °C, while diffusion is the predominant mechanism in the 600–900 °C range. Gonzalez-Julian et al. [31] studied the oxidation resistance of porous Cr_2AlC MAX phase in the total porosity range of 35–75 vol%, prepared using the sacrificial template technique. Cr_2AlC foams were oxidized from room temperature to 800, 900, 1000, 1100, 1200, and 1300 °C, with a heating rate of 10 °C·min^{-1} and a dwelling time of 1 h. They exhibited negligible oxidation rates up to 800 °C, and oxidation resistance remained excellent up to 1300 °C owing to thin and continuous protective outer layer of α-Al_2O_3 formed in situ when temperature reached 900 °C. The α-Al_2O_3 protective layer covered the entire external surface of the pores seamlessly, significantly reducing the rate of subsequent oxidation of the foams. In this work, the oxidation kinetics of highly porous (87 vol%) Ti_2AlC material was investigated for the first time using a continuous thermogravimetric method under steady-state isobaric–isothermal conditions. Ti_2AlC-based cellular structures that have optimized morphology exhibit a number of desirable features. Their permeability, specific/geometric surface area, and refractoriness are all high, and they also have good mechanical strength. They thereby meet a number of prerequisites for widespread adoption in a number of applications, such as hot gas filters, solid/liquid separation devices, catalyst supports, and solar volumetric collectors. In order to these materials be viable for such applications, it is necessary to determine their oxidation resistance at high temperatures. The reason why this particular preparation method was selected is that in gel-casting, the foam is deposited directly and then, immediately consolidated while still wet; foam produced in this way exhibits higher strength than replica ones, even given the same porosity level. This is because of dense struts without voids and cracks [32]. The microstructure, mechanical properties, thermal conductivity, and gas permeability of Ti_2AlC gel-cast foams were described in our previous papers [24–27].

Materials and methods

Preparation of Ti_2AlC foams

Ceramic suspensions of Ti_2AlC powder ($d_{10} = 2.1$, $d_{50} = 12.1$, and $d_{90} = 28.4$ µm, SSA = 1.63 m^2 g^{-1}, Beijing Thai ZhiHui Technology Co., Ltd, China) were prepared with a solid loading of 35 vol% via dispersion in 1.0 mass% of polyacrylic acid (Aldrich, Cat. No. 323667), as proposed by Sun et al. [23]. The Ti_2AlC suspensions were homogenized in a container with alumina balls placed in planetary mill. The applied gelling agent was agarose, which forms a strong gel that is capable of supporting the mass of the foam mass, as described previously [24]. Agarose solutions (2.5 mass%) were synthesized via mixing agarose powder (MEEO Ultra-Qualitat, Roth, Germany) and distilled water, and subsequently, heating the mixture at 95 °C for 1 h.35 vol% Ti_2AlC slurry was added to the agarose solution, while maintaining a temperature of 60 °C. After that process, 25.9 vol% Ti_2AlC was present in the ceramic suspension. 0.60 mass% active gelling matter content was observed in the final slurry with

respect to the dry ceramic powder concentration, which corresponds to 0.87 mass% agarose in regards to the total water content in the slurry. Non-ionic surfactants (Tergitol TMN-10, Sigma-Aldrich, Poznań, Poland, and Simulsol SL-26, Seppic, Puteaux, France) were inserted into the mixture in order to stabilize the foams at 0.8 mL–100 mL^{-1} concentration in the slurry. Agitation was used to perform the foaming process at 60 °C with the help of a double-blade mixer operating at a velocity of 500 rpm for 5 min. duration. The agarose-containing foamed suspension was subsequently poured into a mold, which was then cooled down via the use of flowing cold water (15 °C) responsible for gelling the wet foam. De-molding of the green bodies was then performed after which they were left to dry under ambient conditions. The sintering procedure was carried out in flowing argon atmosphere (99.99% Ar) at 1400 °C. The soaking time was 4 h, and the heating rate up to 650 °C was 1 °C min^{-1}. After that, a rate of 2 °C min^{-1} was applied until the sintering temperature was achieved. The amount of decomposed Ti_2AlC phase during the high-temperature heat treatment was minimized by inserting the foam samples into an alumina boat on an Al-containing MAX-phase powder (Ti_3AlC_2) bed, in accordance with the research of Lu et al. [33].

Characterization methods

The phases formed after sintering as well as those after high-temperature oxidation tests were investigated using X-ray diffraction (PANaticalX'Pert Pro PW 3710 diffractometer, Malvern, UK). XRD measurements were performed using finely ground foams with monochromatic CuKα radiation, within a 2-theta range of 8–85°, with a step size of 0.05°, and a step time of 2 s. The same amount of each sample was analyzed. The HighScore Plus application in conjunction with the software used to operate the X'Pert diffractometer and the ICDD database was used for phase identification.

As specified in ASTM C20-00, the water immersion method based on Archimedes' principle was applied to determine the relative density and open porosity. The reference value applied for the calculation of the total volume fraction of porosity was the helium density of finely ground Ti_2AlC foams, i.e., 4.05 g cm^{-3} (AccuPyc 1340).

The morphology of the produced foams, as well as the foams after oxidation tests was observed via scanning electron microscopy (FEI field emission gun (Schottky emitter)—Nova NanoSEM 200, FEI Europe, Eindhoven, the Netherlands—equipped with an add-on for the energy-dispersive X-ray analysis (EDX) of the chemical composition, manufactured by Genesis Spectrum, Mahwah, NJ, USA. The average cell and cell window size were measured using the linear intercept method (ASTM E112-12),with an image analysis program (Axio Vision LE).

The specific surface area (SSA) of the Ti_2AlC foams was determined using the BET method (ASAP 2020, V304H, with krypton as the adsorptive).

Continuous isothermal oxidation kinetics tests were performed in laboratory air at 600, 700, 800, 900, and 1000 °C for a duration of 3–7 h, using thermogravimetric equipment with the MK2 Vacuum Microbalance Head (CI Electronics Ltd., UK) with a sensitivity of 10^{-7} g. The relative humidity of laboratory air was 35%, which corresponds to absolute humidity of 6.4 g m^{-3} (Professional hygrometer: Delta DHM HD2301.0, MERA, Warsaw, Poland).

Results and discussion

Characterization of Ti_2AlC foams

Figure 1 presents the XRD diffraction patterns of the starting Ti_2AlC commercial powder and the sintered Ti_2AlC gel-cast foam.

The fraction of every phase was determined by normalizing the intensity of the highest XRD peaks for each of them. The composition of the powders was as follows: Ti_2AlC = ~ 89.3%, Ti_3AlC_2 = ~ 11.6%, and TiC = ~ 0.3%. On the other hand, the gel-cast foams after 4 h of sintering at 1400 °C consisted of the following phases: Ti_2AlC = ~ 71.3%, Ti_3AlC_2 = ~ 26.8%, and TiC = ~ 1.9%.

The change in the phase composition of Ti_2AlC powders as a result of high-temperature sintering was caused by the decomposition of Ti_2AlC into Ti_3AlC_2 and TiC [34]. In a highly porous foam, decomposition is likely to be more pronounced than for fully dense samples because of the high surface area of the former. However, it was shown by Lu

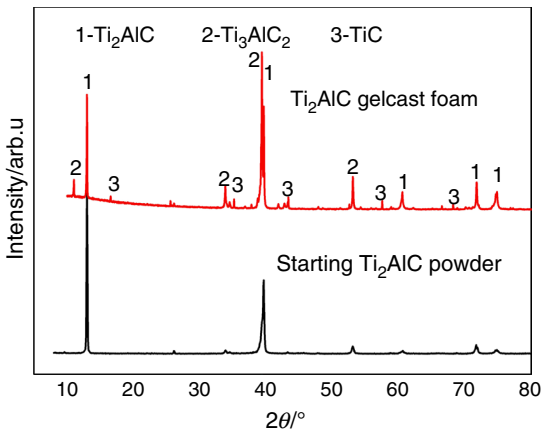

Fig. 1 XRD patterns of the starting Ti_2AlC powder and a gel-cast Ti_2AlC foam with a total porosity of 87 vol%. Phases identified according to the following Inorganic Crystal Structure Database (ICSD) collection codes: 165,460—Ti_2AlC, 153,266—Ti_3AlC_2, and 44,494—TiC

et al. as well as in our previous study that placing porous samples on a Ti_3AlC_2 powder bed while sintering allows a large amount of the Ti_2AlC phase to be retained in the final ceramic foams [24, 33]. Moreover, a Ti_3AlC_2 powder bad minimizes the amount of TiC in the Ti_2AlC MAX-phase foam during heat treatment procedure. The reason is that a Ti_3AlC_2 powder bad offers an Al-rich atmosphere at high temperatures to prevent Ti_3AlC_2 phase in the foam from decomposition to TiC [24, 33].

The supplied Ti_2AlC MAX-phase 211 powders are not entirely homogeneous in terms of composition; in fact, they include considerable amounts of the Ti_3AlC_2 312 MAX phase and minor amounts of a non-MAX phase, namely TiC. Although according to the literature the oxidation behavior of Ti_3AlC_2 at high temperatures (900–1400 °C) is excellent and not that different from the behavior of Ti_2AlC, by all accounts, the oxidation resistance of TiC is poorer—the temperatures at which the oxidation of this phase starts and ends are much lower than the corresponding temperatures for Ti_3AlC_2 [11, 35–38].

Table 1 Total porosity, open porosity, water absorption, bulk density, and specific surface area of Ti_2AlC foams after sintering at 1400 °C

Total porosity/ vol%	Open porosity, vol%	Water absorption/ mass%	Bulk density/g cm^{-3}	Specific surface area/ $m^2\ g^{-1}$
87.1 ± 0.6	86.8 ± 0.4	172 ± 11	0.52 ± 0.03	0.14 ± 0.01

The relative density, open porosity, water absorption, and specific surface area of Ti_2AlC foams after sintering at 1400 °C are listed in Table 1.

The data indicate that the applied processing conditions yielded foams with a total porosity of 87.1 vol%, an open porosity of 86.8 vol%, and interconnected pores; the difference between total and open porosity is less than 1 vol%. The specific surface area (SSA) of the foam with 87.1 vol% of total porosity is low (0.14 $m^2\ g^{-1}$), as was the SSA of the starting powder (1.63$m^2\ g^{-1}$).

The foams consisted mostly of approximately spherical cells that were interconnected with circular windows (Fig. 2a). Image analysis indicated that the foams had a mean cell and cell window size of 335 ± 138 and 72 ± 31 µm, respectively, and a mean strut thickness of 51 ± 19 µm. Spherical pores were associated with polycrystalline struts that still contained some pores that ranged from 0.9 to 3 µm in size (Fig. 2b). Figure 2c shows the Ti_2AlC strut morphology, which featured grains that ranged from less than 1 µm–10 µm; the grains themselves had and a layered internal structure.

The morphology of polycrystalline struts (Fig. 2b) is similar to that manufactured by Sun et al. for dense Ti_3AlC_2 MAX phase that had obtained via slip casting and pressureless sintering at 1420 °C [39].

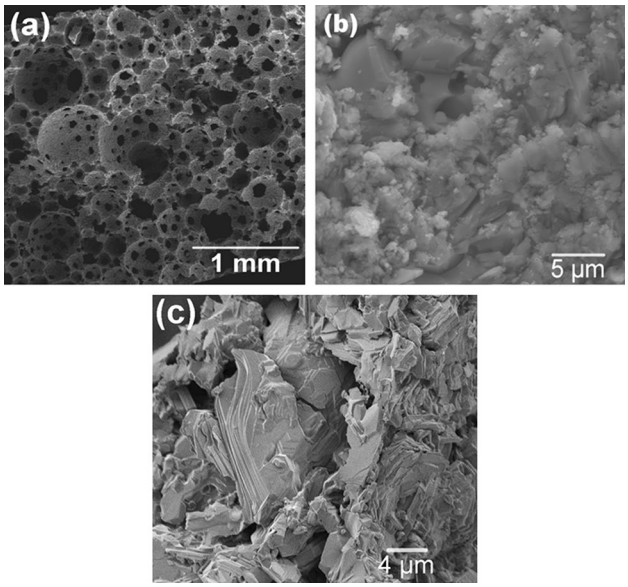

Fig. 2 SEM micrographs of Ti_2AlC foams with a total porosity of 87 vol%: **a** overall view of the foam, **b** typical strut morphology, and **c** typical nano-laminated structure

Oxidation kinetics of Ti_2AlC foams

For bulk Ti_2AlC or Ti_3AlC_2, the mass gain $\left(\frac{\Delta m}{A}\right)$ vs. time kinetics are parabolic or cubic in the temperature range of 900–1300 °C, as represented by Eqs. (1) and (2) [10, 35–37]:

$$\left(\frac{\Delta m}{A}\right)^2 = k_p \cdot t + C_1 \quad (1)$$

$$\left(\frac{\Delta m}{A}\right)^3 = k_c \cdot t + C_2 \quad (2)$$

where $\left(\frac{\Delta m}{A}\right)$—mass gain per unit surface area, k_p, k_c—parabolic or cubic rate constants, t—oxidation time, and C_1,C_2—integration constants defining the onset of parabolic or cubic kinetics, respectively.

On the other hand, the oxidation of MAX phase powders was expressed via the change in the sample mass percentage $\left(\frac{\Delta m}{m_o}\%\right)$ during oxidation time, where Δm is mass gain after oxidation, and m_o is the initial mass of the sample [29, 30]. The foam area was calculated based on the specific surface area of the foam and the foam mass (see previous section). Since the specific surface area of ceramic or metallic foams cannot always be defined accurately, the mass gain of the sample was expressed in two ways: (i) relative to the initial

mass of the sample (Fig. 3), and (ii) relative to the initial foam surface (Fig. 4). This allowed the oxidation kinetics to be determined and made it possible to compare the oxidation rate of the foam with the data for reported for bulk Ti_2AlC and Ti_2AlC_3 in the literature [35–37].The evolution of $\left(\frac{\Delta m}{m_o}\%\right)$ as a function of oxidation time over the temperature range of 600–1000 °C is shown in Fig. 3.

In the 600–800 °C, temperature range sample mass changed only slightly (13.1% at 800 °C), while significant mass gains were observed at 900 and 1000 °C (52.4% at 1000 °C). The Ti_2AlC skeleton was fully oxidized after 1.5 h of oxidation at 1000 °C. This time is much longer than what had been reported by Zhang et al. and Kong et al. for the full oxidation of Ti_2AlC powders (less than 10 min) [29, 30]. The 52.4% increase in $\left(\frac{\Delta m}{m_o}\%\right)$ after oxidation at 1000 °C is highly consistent with the theoretical increases in mass percentage after the full oxidation of Ti_2AlC (56.4%), Ti_3AlC_2 (49.3%), and TiC (33.4%), assuming TiO_2 and Al_2O_3 as the oxidation products [29]. The mass increase at 600 °C is anomalously high—even higher than at 700 °C. This phenomenon was also observed by other authors [29, 40–42] with respect to both Ti_2AlC powders and bulk Ti_2AlC, Ti_3AlC_2, and TiC, and it is discussed in detail in Sect. "XRD, EDS and morphology of Ti2AlC foams".

Mass gain per unit surface area of the Ti_2AlC foam as a function of oxidation time in the temperature range of 600–1000 °C is shown in Fig. 4 (parabolic plot). The parabolic plot fits the straight line best in the temperature range of 600–1000 °C. Figure 4 shows intentionally separated into Fig. 4a, b to clearly show the anomalous nature of oxidation at 600 °C. Not only was the mass gain greater at 600 °C than at 700 °C (Fig. 4a), but it was also intermittent. Since the Ti_2AlC foam was fully oxidized at 1000 °C, the parabolic rate constant for this temperature was calculated for the first 45 min of the reaction, after which the mass gain reached a plateau (Fig. 4b).

Figure 5 shows how the oxidation data determined in this work for the Ti_2AlC foam compares with the literature data for dense Ti_2AlC and Ti_3AlC_2 MAX phases. The oxidation kinetics of Ti_2AlC foams was characterized by low parabolic rate constants, indicating very good resistance to oxidation at high temperatures, especially given the fact that this material had the form of a highly porous foam. The parabolic rate constants of the Ti_2AlC foam were about one and half order of magnitude higher than that of bulk Ti_2AlC [35] and one order of magnitude higher than those reported for bulk Ti_3AlC_2 MAX phases [36, 37]. This comparison is valid for 900 and 1000 °C, because the relevant data on Ti_2AlC and Ti_3AlC_2 oxidation had only been reported for higher temperatures (900–1400 °C). It should be noted that the kinetics data presented in Fig. 5 are valid for brief oxidation

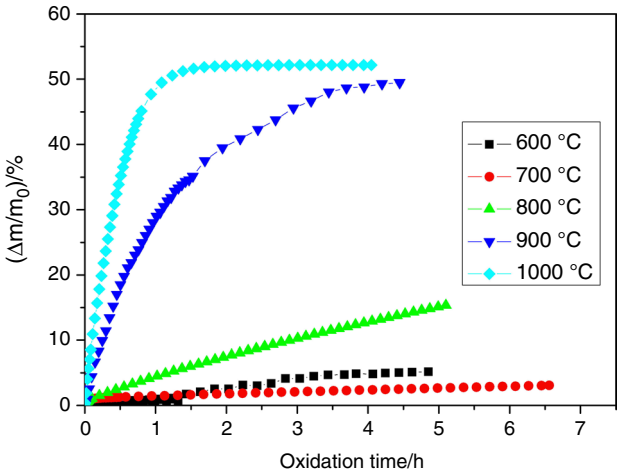

Fig. 3 Mass gain per initial sample mass of a Ti_2AlC foam with 87 vol% of total porosity as a function of oxidation time in static air at temperatures in the range of 600–1000 °C

times, and more data on the long-term oxidation behavior of Ti_2AlC foams will be obtained as part of subsequent studies.

XRD, EDS and morphology of Ti_2AlC foams

Phase changes in Ti_2AlC specimens resulting from oxidation in static air in the temperature range 600–1000 °C were initially determined by means of XRD analysis (Fig. 6). After being subjected to air atmosphere at 600 °C, a weak anatase (011) peak at 25.3° can be observed. Moreover, aTi_2AlC signature peak at 12.9° now has lower intensity. This suggests a decrease in Ti_2AlC phase mass fraction inside the foam as a result of the oxidation process. This decline in peak intensity is proportional to temperature and disappears in the 900–1000 °C range. Although the transformation from anatase to rutile usually occurs in the 600–700 °C temperature range, no rutile peaks were detectable in samples oxidized below 800 °C. The reasons are probably kinetic factors resulting from short oxidation time and low reaction rate.

After oxidation at 800 °C, rutile (110) and (211) peaks could be determined at 27.5 and 54.5°. The intensity of the afore-mentioned rutile TiO_2 peaks increased at 900 °C, which implies higher rutile TiO_2 concentration. It should be emphasized that, due to the relatively short oxidation duration (several hours), transition aluminum oxides (e.g., γ- or β-Al_2O_3) were not observed. Rutile TiO_2 and corundum Al_2O_3 diffraction peaks were determined after exposure to air at 1000 °C, indicating full oxidation of the investigated Ti_2AlC foams. A weak peak of FeO ($2\theta = 42.2°$) at after oxidation at 1000 °C came from the sample holder.

The intensities of the peaks originating from rutile were much higher than those from Al_2O_3. The XRD results obtained in this work are in good agreement with those

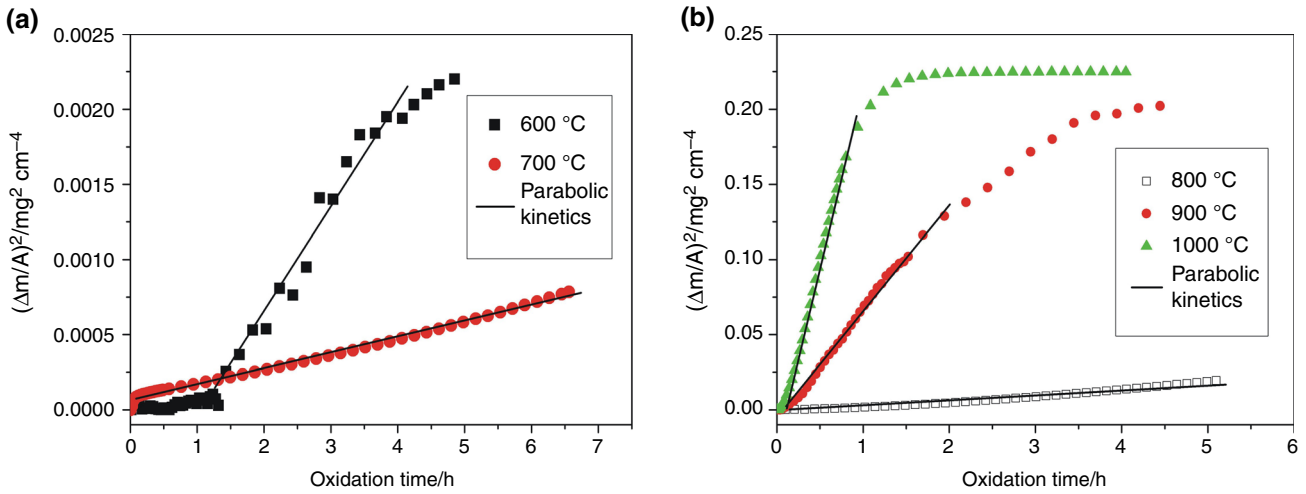

Fig. 4 Mass gain per unit surface area of a Ti_2AlC foam with 87 vol% of total porosity as a function of oxidation time in the temperature range of 600–700 °C **a** and 800–1000 °C **b**, with air as the oxidizing atmosphere (parabolic plot)

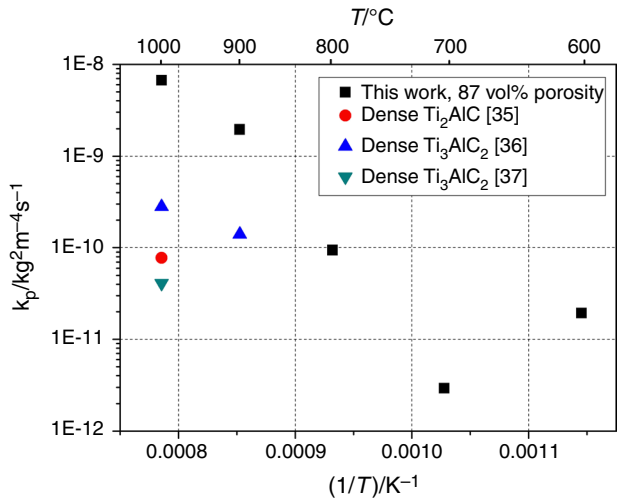

Fig. 5 Comparison of k_p (parabolic rate constant, $kg^2\ m^{-4}\ s^{-1}$) values determined for the oxidation of Ti_2AlC foams with 87 vol% of total porosity and the literature data for denseTi_2AlC and Ti_3AlC_2 MAX phases (Arrhenius plot)

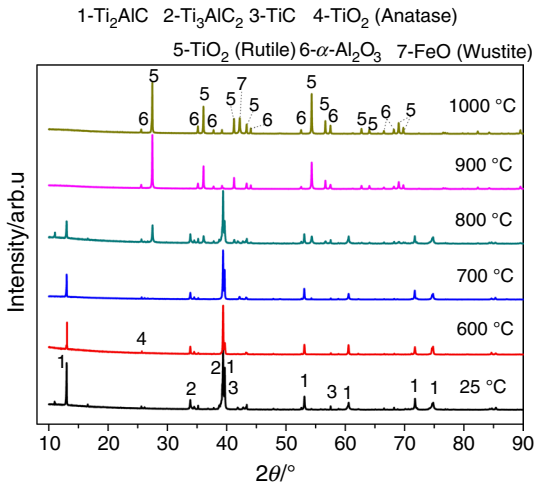

Fig. 6 XRD patterns recorded for Ti_2AlC foams after oxidation in static air at temperatures between 600 and 1000 °C

reported by Zhang et al., who studied the oxidation of Ti_2AlC powders in the temperature range between 200 and 1000 °C [29].

Morphological observations showed that the microstructure of the Ti_2AlC foam was retained after oxidation in the temperature range of 600–1000 °C. As shown in Fig. 7, the cells and cell windows of the foam are visible after oxidation at all temperatures, although a small reduction in window size was observed, especially after oxidation at 1000 °C.

However, the nature of the scale formed on the strut surface of the Ti_2AlC foams changed significantly depending on oxidation temperature. As mentioned earlier, the oxidation kinetics at 600 °C should be considered abnormal. The performed SEM observations confirmed this behavior—after oxidation at this temperature the foam surface featured gaps/cracks between the Ti_2AlC layers, and fine plate-like oxide crystals had nucleated on it (Fig. 7a). The EDS results showed the oxidation products to be mixed Ti and Al oxides. The gaps/cracks were likewise observed after oxidation of bulk Ti_2AlC [40] and bulk Ti_3AlC_2 [41] at 600 °C as well as bulk TiC at 400 °C [38]. Wang and Zhou [40] attributed such cracks to the stress resulting from the volume expansion associated with the oxidation of Ti_2AlC to anatase. Conversely, according to [29, 42–44], Ti_2AlC partial oxidation is responsible for the anomalous oxidation behavior determined at 600 °C, as well as incorporation of oxygen atoms into Ti_2AlC, resulting in an O-doped Ti_2AlC MAX phase and Ti_2AlC_{1-x} oxycarbide. Further, oxidation leads to TiO_2

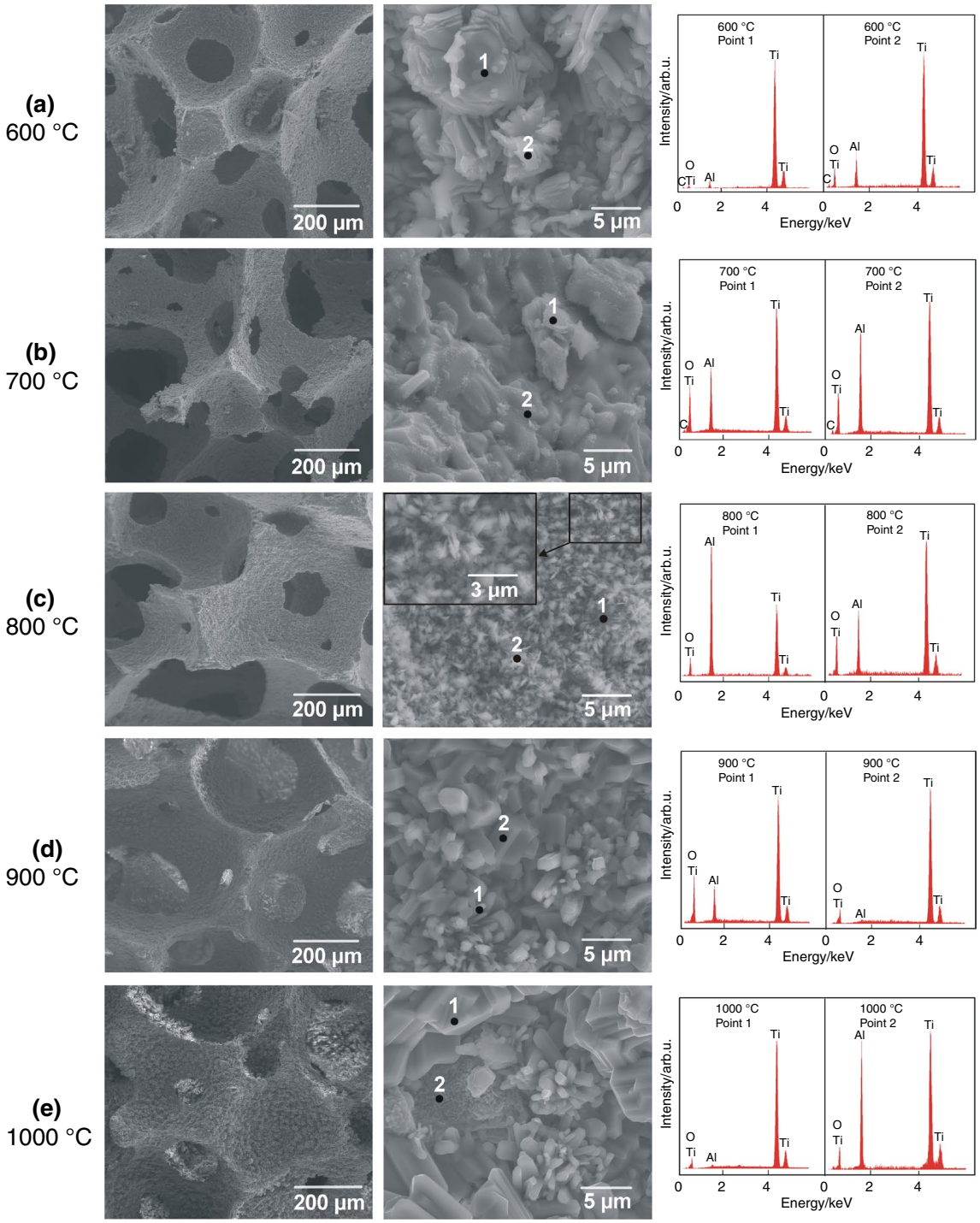

Fig. 7 Morphology and EDS analysis of Ti_2AlC foams after oxidation at each of the following temperatures: **a** 600 °C, **b** 700 °C, **c** 800 °C, **d** 900 °C, and **e** 1000 °C

and Al_2O_3 growth, during which C is lost due to CO_2 formation. The morphology of the scale formed after oxidation at 700 °C was noticeably different from that observed at 600 °C (Fig. 7b). The scale grains were integrated, indicating that the scale had protective properties and allowed a smaller amount of oxidation products to form, which is consistent with the oxidation kinetics. The oxidation products consisted of fine oxide grains (< 1 μm). The EDS results revealed that the oxidation products were mixed Ti and Al oxides. The oxide scale formed at 800 °C was composed of mixed TiO_2 and Al_2O_3 oxides in the shape of fine plate-like grains or whiskers (Fig. 7c). The oxidation behavior of Ti_2AlC foams

at 800 °C was much like that described in the literature for Ti–Al alloys, for which no protective Al_2O_3 layer was observed when Al content was below a certain threshold; instead, scales composed of TiO_2 and Al_2O_3 had formed [45–47]. After oxidation at 900 °C, the foam was covered by an oxide scale composed of elongated TiO_2 plates and small, mixed Ti and Al oxides (Fig. 7d). The oxide scale formed at 1000 °C was composed of large TiO_2 grains and small Al_2O_3 ones (Fig. 7e). In the temperature range of 900–1000 °C, TiO_2 grains were much larger than the Al_2O_3 ones, indicating that TiO_2 grew faster than Al_2O_3.

Conclusions

The isothermal oxidation behavior of highly porous gel-cast Ti_2AlC foams with a total porosity of 87 vol% was investigated in temperature range of 600–1000 °C, and it was found that this process obeyed the parabolic rate law. The determined parabolic oxidation rate constants were low, indicating that the material's resistance to oxidation at high temperatures was very good, especially given its highly porous form. The parabolic rate constants determined when oxidizing the Ti_2AlC foam at 900 and 1000 °C were about one order of magnitude higher than those reported in the literature for bulk Ti_2AlC and Ti_2AlC_3.

The conducted XRD and SEM/EDS investigations revealed complex differences in scale morphology depending on the oxidation temperature. Ti and Al oxides were the only corrosion products detected after oxidation at 600 and 700 °C. For 800–1000 °C, Al_2O_3 and rutile were detected, with TiO_2 having a higher mass fraction than Al_2O_3.

Acknowledgements Financial support from Rzeszow University of Technology, Poland (PB25.CM.22.001) is gratefully acknowledged. The authors want to acknowledge the X-ray Diffraction Laboratory at the Faculty of Materials Science and Ceramics of AGH University of Science and Technology (Dr Anna Adamczyk) in Krakow, Poland for X-ray diffraction measurements.

Author contributions All authors contributed to the study conception and design. Material preparation, data collection, and analysis were performed by MP, JD, and TB. The first draft of the manuscript was written by MP, and all authors commented on previous versions of the manuscript. All authors read and approved the final manuscript.

Declarations

Conflict of interest This work does not have any conflicts of interest.

References

1. Barsoum MW. MAX phases: properties of machinable ternary carbides and nitrides. Weinheim Germany: Viley-VCH Verlag GmbH; 2013.
2. Radovic M, Barsoum MW. MAX phases: bridging the gap between metals and ceramics. Am Ceram Soc Bull. 2013;92:20–7.
3. Sun ZM. Progress in research and development on MAX phases: a family of layered ternary compound. Int Mater Rev. 2011;56:143–66. https://doi.org/10.1179/1743280410Y.0000000001.
4. Barsoum MW, Radovic M. Elastic and mechanical properties of the MAX phases. Ann Rev Mater Res. 2011;41:195–227. https://doi.org/10.1146/annurev-matsci-062910-100448.
5. Lapauw T, Swarnakar AK, Tunca B, Lambrinou K, Vleugels J. Nanolaminated ternary carbide (MAX phase) materials for high temperature applications. Int J Refract Met Hard Mater. 2018;72:51–5. https://doi.org/10.1016/j.ijrmhm.2017.11.038.
6. Sundberg M, Malmqvist G, Magnusson A, El-Raghy T. Alumina forming high temperature silicides and carbides. Ceram Int. 2004;30:1899–904.
7. Gupta S, Filimonov D, Zaitsev V, Palanisamy T, Barsoum MW. Ambient and 550°C tribological behavior of selected MAX phases against Ni-based superalloys. Wear. 2008;264:270–8.
8. Barnes LA, Rago NLD, Leibowitz LJ. Corrosion of ternary carbides by molten lead. J Nucl Mater. 2008;373:424–8. https://doi.org/10.1016/j.jnucmat.2007.04.054.
9. Wang XH, Zhou YC. Layered machinable and electrically conductive Ti_2AlC and Ti_3AlC_2 ceramics A Review. J Mater Sci Technol. 2010;26:385–416. https://doi.org/10.1016/S1005-0302(10)60064-3.
10. Smialek JL. Oxidation of Al_2O_3 scale-forming MAX phases in turbine environments. Metall Mater Trans A Phys Metall Mater Sci. 2017;49:782–92. https://doi.org/10.1007/s11661-017-4346-9.
11. Tallman DJ, Anasori B, Barsoum MW. Critical review of the oxidation of Ti_2AlC, Ti_3AlC_2 and Cr_2AlC in Air. Mater Res Lett. 2013;1:115–25. https://doi.org/10.1080/21663831.2013.806364.
12. Smialek JL. Oxygen diffusivity in alumina scales grown on Al-MAX phases. Corr Sci. 2015;91:281–6. https://doi.org/10.1016/j.corsci.2014.11.030.
13. Yu W, Vallet M, Levraut B, Gauthier-Brunet V, Dubois S. Oxidation mechanisms in bulk Ti_2AlC: influence of the grain size. J Eur Ceram Soc. 2020;40:1820–8. https://doi.org/10.1016/j.jeurceramsoc.2020.01.042.
14. Xu L, Zhu D, Liu Y, Suzuki TS, Kim B, Sakka Y, et al. Effect of texture on oxidation resistance of Ti_3AlC_2. J Eur Ceram Soc. 2018;38:3417–23. https://doi.org/10.1016/j.jeurceramsoc.2018.03.009.
15. Yang HJ, Pei YT, Rao JC, de Hosson JTM, Li SB, Song GM. High temperature healing of Ti_2AlC: on the origin of in homogeneous oxide scale. Scr Mater. 2011;65:135–8.
16. Velasco B, Gordo E, Tsipas SA. MAX phase Ti_2AlC foams using a leachable space-holder material. J Alloys Compd. 2015;646:1036–42. https://doi.org/10.1016/j.jallcom.2015.05.235.

17. Bowen CR, Thomas T. Macro-porous Ti_2AlC MAX-phase ceramics by the foam replication method. Ceram Int. 2015;41:12178–85. https://doi.org/10.1016/j.ceramint.2015.06.038.
18. Firstov SA, Gorban VF, Ivanova II, Pechkovskii EP. Mechanical properties of porous Ti_3SiC_2/TiC and Ti_4AlN_3/TiN nanolaminate sat 20 to 1300°C. Powder Metall Met Ceram. 2010;49:414–23. https://doi.org/10.1007/s11106-010-9252-2.
19. Gonzales-Julian J. Processing of MAX phases: from synthesis to applications. J Am Ceram Soc. 2021;104:659–90. https://doi.org/10.1111/jace.17544.
20. Hu L, Benitez R, Basu S, Karaman I, Radovic M. Processing and characterization of porous Ti_2AlC with controlled porosity and pore size. Acta Mater. 2012;60:6266–77. https://doi.org/10.1016/j.actamat.2012.07.052.
21. Hu L, Karaman I, Radovic M. Simple, inexpensive synthesis of damage tolerant MAX phase foams. Am Ceram Soc Bull. 2013;92:31–2.
22. Zhou CI, Ngai TVL, Lu L, Li YY. Fabrication and characterization of pure porous Ti_3SiC_2 with controlled porosity and pore features. Mater Lett. 2014;131:280–3. https://doi.org/10.1016/j.matlet.2014.05.198.
23. Sun Z, Liang Y, Li M, Zhou Y. Preparation of reticulated MAX phase support with morphology-controllable nanostructured ceria coating for gas exhaust catalyst devices. J Am Ceram Soc. 2010;93:2591–7. https://doi.org/10.1111/j.1551-2916.2010.03776.x.
24. Potoczek M, Guzi de Moraes E, Colombo P. Ti_2AlC foams produced by gel-casting. J Eur Ceram Soc. 2015;35:2445–52. https://doi.org/10.1016/j.jeurceramsoc.2015.03.015.
25. Elsayed H, Chmielarz A, Potoczek M, Fey T, Colombo P. Direct ink writing of three dimensional Ti_2AlC porous structures. Addit Manuf. 2019;28:365–72. https://doi.org/10.1016/j.addma.2019.05.018.
26. Potoczek M, Chmielarz A, Innocentini MDM, Silva ICP, Colombo P, Winiarska B. Porosity effect on microstructure, mechanical and fluid dynamic properties of Ti_2AlC by direct foaming and gel-casting. J Am Ceram Soc. 2018;101:5346–57. https://doi.org/10.1111/jace.15802.
27. Fey T, Stumpf M, Chmielarz A, Colombo P, Greil P, Potoczek M. Microstructure, thermal conductivity and simulation of elastic modulus of MAX-phase (Ti_2AlC) gel-cast foams. J Eur Ceram Soc. 2018;38:3424–32. https://doi.org/10.1016/j.jeurceramsoc.2018.04.012.
28. Tsipas SA, Tabares E, Weissgaerber T, Hutsch T, Sket F, Velasco B. Thermophysical properties of porous Ti_2AlC and Ti_3SiC_2 produced by powder metallurgy. J Alloys Compd. 2021;857:158145. https://doi.org/10.1016/j.jallcom.2020.158145.
29. Zhang Z, Lim SH, Lai DMY, Tan SY, Koh XQ, Chai J, Wana SJ, Jin H, Pan JS. Probing the oxidation behavior of Ti_2AlC MAX phase powders between 200 and 1000 °C. J Eur Ceram Soc. 2017;37:43–51. https://doi.org/10.1016/j.jeurceramsoc.2016.08.004.
30. Kong F, Feng K, Bai Y, Li N, Qi X, Zheng Y, Wang R, He X. Oxidation behavior of high-purity nonstoichiometric Ti_2AlC powders in flowing air. J Mater Res. 2017;32:2747–54. https://doi.org/10.1557/jmr.2017.83.
31. Gonzalez-Julian J, Onrubia S, Bram M, Broeckmann C, Vassen R, Guillon O. High temperature oxidation and compressive strength of Cr_2AlC MAX phase foams with controlled porosity. J Am Ceram Soc. 2018;101:542–52. https://doi.org/10.1111/jace.15224.
32. Innocentini MDM, Sepulveda P, Salvini VR, Pandolfelli VC. Permeability and structure of cellular ceramics: a comparison between two preparation techniques. J Am Ceram Soc. 1998;81:3349–52. https://doi.org/10.1111/j.1151-2916.1998.tb02782.x.
33. Lu X, Zhou Y. Pressureless sintering and properties of Ti_3AlC_2. Int J Appl Ceram Technol. 2010;7:744–51. https://doi.org/10.1111/j.1744-7402.2009.02403.x.
34. Spencer CB, Cordoba JM, Obando N, Sakulich A, Radovic M, Oden M, et al. Phase evaluation in Al_2O_3 fiber-reinforced Ti_2AlC during sintering in the 1300 °C–1500 °C temperature range. J Am Ceram Soc. 2011;94:3327–34. https://doi.org/10.1111/j.1551-2916.2011.04612.x.
35. Wang XH, Zhou YC. High-temperature oxidation behavior of Ti_2AlC in Air. Oxid Met. 2003;59:304–20. https://doi.org/10.1023/A:1023092027697.
36. Wang XH, Zhou YC. Oxidation behavior of Ti_3AlC_2 at 1000–1400°C in air. Corr Sci. 2003;45:891–907. https://doi.org/10.1016/S0010-938X(02)00177-4.
37. Xuewen X, Yangxian L, Bingchu M, Jiaoqun Z, Heyan L, Jingping Q. Study on the isothermal oxidation behavior in air of Ti_3AlC_2 sintered by hot pressing. Sci China Ser E. 2006;49:513–20. https://doi.org/10.1007/s11431-006-0513-8.
38. Shimada S, Kozeki M. Oxidation of TiC at low temperatures. J Mater Sci. 1992;27:1869–75. https://doi.org/10.1007/BF01107214.
39. Sun Z, Li M, Hu L, Lu X, Zhou Y. Surface chemistry, dispersion behavior, and slip casting of Ti_3AlC_2 suspensions. J Am Ceram Soc. 2009;92:1695–702. https://doi.org/10.1111/j.1551-2916.2009.03136.x.
40. Wang XH, Zhou YC. Intermediate-temperature oxidation behavior of Ti_2AlC in air. J Mater Res. 2002;17:2974–3071. https://doi.org/10.1557/JMR.2002.0431.
41. Wang XH, Zhou YC. Oxidation behavior of Ti_3AlC_2 powders in flowing air. J Mater Chem. 2002;12:2781–5. https://doi.org/10.1016/S0010-938X(02)00177-4.
42. Dahlqvist M, Alling B, Abrikosov IA, Rosen J. Phase stability of Ti_2AlC upon oxygen incorporation: a first-principles investigation. Phys Rev B. 2010;8:024111. https://doi.org/10.1103/PhysRevB.81.024111.
43. Liao T, Wang J, Li M, Zhou Y. First-principles study of oxygen incorporation and migration mechanisms in Ti_2AlC. J Mater Res. 2009;24:3190–6. https://doi.org/10.1557/jmr.2009.0377.
44. Persson POA, Rosen J, McKenzie DR, Bilek MMM. Formation of the MAX-phase oxycarbide $Ti_2AlC_{1-x}O_x$studied via electron energy-loss spectroscopy and first-principles calculations. Phys Rev B. 2009;80:092102. https://doi.org/10.1103/PhysRevB.80.092102.
45. Meier GH, Pettit FS, Hu S. Oxidation behavior of titanium aluminides. J Phys IV. 1993;3:395–402. https://doi.org/10.1051/jp4:1993941.
46. Shida Y, Anada H. The effect of various ternary additives on the oxidation behavior of Ti-Al in high-temperature air. Oxid Met. 1996;45:197–219. https://doi.org/10.1007/BF01046826.
47. Rahmel A, Schütze M, Quadakkers WJ. Fundamentals of TiAl oxidation—a critical review. Mater Corros. 1995;46:271–85. https://doi.org/10.1002/maco.19950460503.